SOVIET PHYSICS USPEKHI VOLUME 9, NUMBER 5 MARCH-APRIL 1967

539.107.49

NEW APPARATUS AND METHODS OF MEASUREMENT

NUCLEAR RADIATION DETECTORS BASED ON IMAGE ITENSIFIERS

M. N. MEDVEDEV

Joint Institute for Nuclear Research

Usp. Fiz. Nauk. 90, 143–161 (September, 1966)

INTRODUCTION

THE passage of charged particles through a scintillator is accompanied by flashes of light arising along the trajectory. The duration of the flashes is determined by the properties of the scintillator and usually is in the range 10^{-5}—10^{-7} sec in inorganic single crystals and 10^{-8}—10^{-9} sec in organic scintillators. The intensity of these flashes does not exceed 10^4—10^6 light quanta per cm of particle path.

If the velocity of the particle is greater than the phase velocity of light in the material, the particles excite flashes of Cerenkov radiation whose duration is of the order of 10^{-10} sec and intensity 1—200 light quanta per cm of path.

Use of image intensifiers permits us in principle to obtain nuclear radiation detectors which record on film not only the particle tracks in scintillators but also the ring from Cerenkov radiation excited by individual charged particles in radiators. These detectors should have continuous sensitivity, high time resolution, and should allow programming of their operation.

One of these detectors—the scintillation chamber—was proposed in 1952 by E. K. Zavoĭskiĭ and coworkers.[1,2] Using as a working medium a crystal of CsI(Tl), the authors photographed proton and slow μ-meson tracks on motion picture film.

In recent years electron-optical image intensifiers have been developed with large entrance photocathodes and high geometrical resolution, and more efficient sources of light pulses excited by charged particles have been produced. This has permitted construction of scintillation chambers and Cerenkov chambers with working volumes of several liters.[6] However, the geometrical resolution of the detectors does not exceed 8—10 line pairs per mm. Further perfection of the image intensifiers is required.

In this review we discuss papers published in the last eight or nine years on nuclear radiation detectors employing image intensifiers, and describe by way of illustration the results of several studies made with these detectors.

I. ELECTRON-OPTICAL IMAGE INTENSIFIERS

Recording on film of the luminous tracks of particles in a scintillator and of rings from Cerenkov radiation is possible only for definite image-intensifier parameters. First of all it is necessary that the image intensifier have a gain of the order of 10^7 and a geometrical resolution of about ten line pairs per mm, i.e., 0.1 mm. In the second place it is necessary that the image amplifiers permit rapid establishment of a steady operating condition with low intrinsic noise. Third, it is necessary that the spectral sensitivity of the entrance photocathode of the image intensifier correspond to the spectral composition of the scintillation flashes and Cerenkov flashes. These requirements are best satisfied by the multistage electron-optical image converters whose construction has been described in [2,7,63]. The principle of operation of the image converter is as follows: an optical image of some object, projected onto the entrance photocathode, is converted to an electronic image and then, by means of an electron-optical system and a fluorescent screen, again converted to a visible image with a spectral composition determined by the phosphor from which the screen is prepared.

In scintillation chambers and Cerenkov detectors the electron-optical converter acts as a brightness amplifier for the optical images of the particle tracks and Cerenkov rings. Therefore in this review we will refer to electron-optical converters as image intensifiers.

The design, principle of operation, and characteristics of single-stage image intensifiers has been described by Eckart[3] and Shcheglov.[8] In scintillation chambers and Cerenkov chambers, single-stage image intensifiers are used only with a large entrance-photocathode surface for converting the dimensions of the optical images of the objects being studied. The geometrical resolution of these amplifiers is 4—6 line pairs per mm and the gain does not exceed 20.[6,8,49]

1. Theory and Design of Multistage Image Intensifiers

Multistage image intensifiers consist of a cylindrical tube in which the amplifier chambers are located. The construction of an intensifier is shown schematically in Figs. 1 and 2.

The intensifier shown in Fig. 1 consists of an entrance chamber and five amplifier chambers. The entrance chamber has a semitransparent photocathode of the end-window type. Beyond the photocathode there is a fluorescent screen deposited on a thin

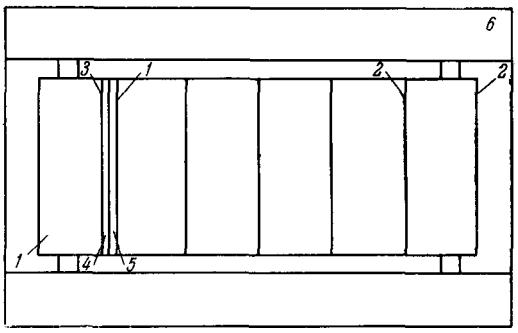

FIG. 1. Block diagram of multistage image intensifier. 1 – photocathode; 2 – fluorescent screen; 3 – aluminum film; 4 – phosphor; 5 – glass or mica; 6 – solenoid.

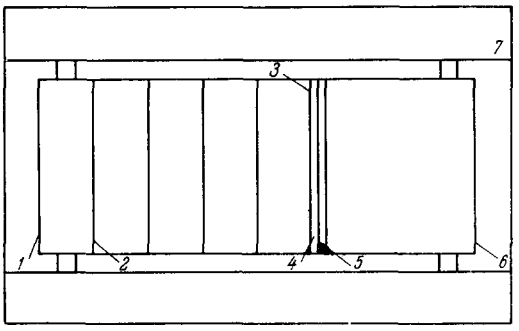

FIG. 2. Block diagram of image intensifier utilizing secondary emission. 1 – photocathode; 2 – screen; 3 – aluminum oxide layer; 4 – aluminum layer; 5 – material with high secondary emission (KCl); 6 – fluorescent screen; 7 – solenoid.

transparent film of glass or mica. On the other side of the film is located the photocathode of the first amplifier chamber. The remaining amplifier chambers are arranged similarly. The fifth amplifier chamber is terminated in a fluorescent screen from which the optical image of the object being studied is photographed.

All of the fluorescent screens are covered with a thin layer of aluminum, since metallization considerably improves the luminous efficiency of the screen and protects it from alkali metals during processing of the photocathodes.[8]

An electron emitted from the entrance photocathode is accelerated by a constant electric field and focused by an axial magnetic field onto the entrance-chamber screen. The electron loses its energy on passing through the phosphor. Part of this energy is radiated by the molecules of the phosphor in the form of photons, which pass through the transparent film and hit the photocathode of the first amplifier chamber. As a result, new electrons appear, etc.

The number of photons produced by one electron depends on the electron energy E, the thickness of the screen, and the phosphor energy output ϵ. Knowing the photocathode quantum efficiency η of the amplifier and the energy $h\nu$ of the photons radiated by the phosphor, we can determine the gain M of one chamber from the expression

$$M=\frac{\eta\varepsilon E}{h\nu}. \qquad (1)$$

For example, an electron accelerated to 15 keV produces, in a phosphor with an energy yield of ~ 10%, up to 500 photons with an energy of 3 eV. This means that with a photocathode quantum efficiency of the order of 10%, the gain of a single chamber can be about 50.

Acceleration of the electrons in the chambers to higher energies is clearly not desirable, since thicker screens are required to absorb them. Increasing the screen thickness results in deterioration of the phosphor transparency for its own radiation and, consequently, in reduction of the gain. Furthermore, increasing the screen thickness spoils the geometrical resolution of the image intensifier, whose chambers are connected by optical contact.

The image amplifiers described by E. K. Zavoĭskiĭ and co-workers[2,9] and other authors[10] permit recording on film of the light flash from a single photoelectron emitted from the entrance photocathode. The geometrical resolution of such amplifiers is 0.1 mm, i.e., one electron emitted by the entrance photocathode excited in the output screen of the intensifier a luminous spot 0.1 mm in diameter.[9] Image intensifiers of this type but with three amplifier chambers have been described by Stoudenheimer et al.[11]

Figure 2 shows schematically an image intensifier employing secondary emission. It consists of six amplifier chambers. The first chamber has a semitransparent photocathode of the end-window type, after which there are five screens. The output chamber is terminated in a fluorescent screen.

An electron emitted from the photocathode is accelerated by an electric field and focused by an axial magnetic field to the screen of the first amplifier chamber. The first screen emits secondary electrons

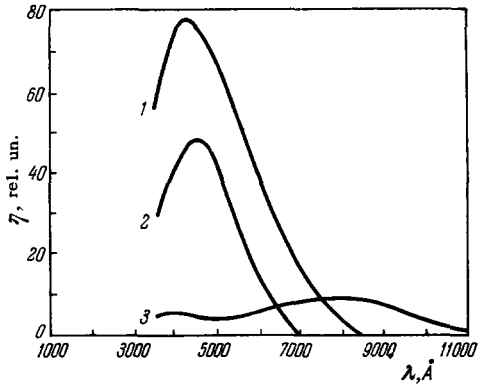

FIG. 3. Relative spectral sensitivity curves of several photocathodes. 1 – multialkali cathode; 2 – antimoni-cesium cathode; 3 – oxygen-cesium cathode.

which are accelerated and hit the second screen, and so forth. In the final chamber the secondary electrons are accelerated and focused onto the fluorescent screen, from which the optical image of the object being studied is photographed.

The intensifier uses screens having a high secondary emission. A screen consists of a film of aluminum oxide 400 Å thick, on which are deposited a conducting layer of aluminum and a 400 Å layer of KCl. The secondary-emission coefficient of KCl depends on the primary electron energy. For example, for 15-keV electrons the secondary-emission coefficient, according to the measurements of several authors,[12,13] is close to 5. Thus the total gain of a secondary-emission image intensifier does not exceed $(1-2)\times 10^5$.[7] However, these gain values are insufficient for recording on film the light flashes excited by a single electron emitted from the entrance photocathode.

The geometrical resolution in intensifiers of this type is determined mainly by the electron velocity and is about 0.07 mm for an electric-field intensity of 10^3 V/cm and a focusing magnetic field of 200—300 G.

The image intensifiers used in nuclear radiation detectors are prepared, as a rule, with antimony-cesium or antimony-sodium-potassium-cesium entrance photocathodes. Figure 3 illustrates the relative spectral sensitivity curves of several photocathodes.

The greatest sensitivity is obtained with the multialkali photocathodes. Their quantum efficiency in the region of maximum sensitivity is about 20%, and some samples considerably exceed this value.[8] In spite of their comparatively high sensitivity in the red region, the dark current of multialkali photocathodes does not exceed that of antimony-cesium photocathodes.

The quantum efficiency of antimony-cesium photocathodes is considerably below that of multialkali photocathodes, but the spectral sensitivity occurs in the region from 3000 to 6000 Å. The dark current of antimony-cesium photocathodes does not depend greatly on temperature. Therefore the amplifier chambers of multistage image intensifiers are in most cases made with antimony-cesium photocathodes.[8]

The output screens of image intensifiers are made mainly from the phosphors ZnS(Ag) or ZnS(Cu), whose geometrical resolution is about 0.05 mm.

2. Intrinsic Noise of Image Intensifiers

Multistage image intensifiers record on film the light flash from a single electron emitted from the entrance photocathode. This means that the threshold intensity of the light flash for detection on the film is determined mainly by the quantum efficiency of the entrance photocathode of the intensifier. High gain leads to unavoidable difficulties—intrinsic intensifier noise which appears in the form of luminous points on the output screen of the intensifier.[2,10,19]

The intrinsic noise of an intensifier is due to the electron dark current arising from thermionic and field emission from the photocathodes and from ion and optical feedback. The main contribution to the electron dark current is thermionic emission from the photocathodes.

The number of thermionic electrons increases rapidly with temperature and can be determined from the expression

$$m = AN^{1/2}T^{5/4}e^{-\varphi_0/kT}, \qquad (2)$$

where A is a constant, N is the concentration of impurity atoms, φ_0 is the work function, T is the temperature, and k is the Boltzmann constant. Thus, for example, from a square cm of surface of antimony-cesium photocathode at room temperature, up to 10^4—10^5 electrons/sec are emitted.[14]

Field emission becomes important for surfaces with a low work function at an electric field intensity of the order of 10^5 V/cm.[15] A field of this strength can arise in the amplifier chambers are the result of irregularities on the photocathode surfaces.[16]

In field emission, electrons are emitted not only from irregularities in the photocathodes but also from individual regions in the photocathode support which are activated by cesium,[17] and from the walls of the tube.[18] Field emission can therefore contribute a large fraction to the total number of dark current electrons.

In some specimens of image intensifiers a diffuse spot of light is observed in the center of the output screen. The nature of this spot of light is evidently connected with bombardment of the photocathodes by ions which knock out substantial groups of secondary electrons. These electrons, focused by the magnetic field onto the fluorescent screens, result in appearance of the spot of light at the output screen.[8]

Quantitative studies of intrinsic noise in multistage image intensifiers with antimony-cesium photocathodes have been made by Zavoĭskiĭ et al.[9]

It has been established by visual observation that the light flashes on the output screen of an intensifier, produced by dark-current electrons from the entrance photocathode, differ not only in size but also in brightness. The weak light flashes with area of the order of 10^{-4} cm^2 are evidently produced by individual electrons, and the brighter flashes by substantial groups of electrons.

In order to study the nature of the multielectron component of the intrinsic noise and to determine the number of electrons in a group, Zavoĭskiĭ et al. used the technique of defocusing the electron image in the entrance chamber of the intensifier. As a result a bright light flash broke up into individual luminous points with roughly the same brightness. This al-

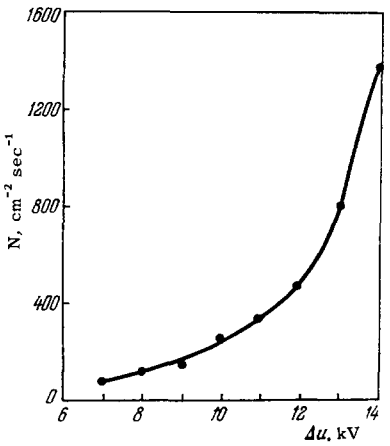

FIG. 4. Number of electron groups as a function of potential difference in the entrance chamber.

lowed determination of the number of electrons in a group, which changed from 2—3 to 15—20 as a function of the field strength in the entrance chamber.

From analysis of the experimental data Zavoĭskiĭ et al. conclude that at room temperature and for a potential difference of 12 kV in the entrance chamber, an antimony-cesium photocathode emits about 20 individual electrons per cm^2 per sec and about 500 localized groups of electrons. Figure 4 shows the number of electron groups N as a function of the potential difference in the entrance chamber.

Thus, in a multistage image intensifier with an antimony-cesium photocathode, the main component of the intrinsic noise is the multielectron component. The number of electron groups does not depend on the temperature of the entrance photocathode and is determined mainly by the potential difference in the entrance chamber.

By decreasing the potential difference in the entrance chamber, the number of electron groups can be considerably reduced. However, in this case there will be a drop in the geometrical resolution of the intensifier, which is determined mainly in the entrance chamber of the intensifier and which depends on the field intensity at the entrance photocathode. Actually, to provide a minimum circle of confusion $\Delta\delta$ in an image intensifier it is necessary that the field intensity U at the photocathode be at least equal to the value given by the expression [8]

$$U = 2L\frac{v_0}{\Delta\delta}, \qquad (3)$$

where L is the distance between the photocathode and the fluorescent screen, and v_0 is the initial energy of the electron. It follows from this expression that the potential difference in the entrance chamber has a lower limit. Therefore the best method of suppressing intrinsic noise due to dark-current electrons in a multistage image intensifier is use of a pulsed supply voltage for the amplifier chambers.

3. Pulse Operation of an Image Intensifier

The dark current electrons are emitted from the entrance photocathode independently of each other. This means that for a light flash duration of 10^{-10}—10^{-8} sec, Cerenkov cones and particle tracks in scintillators can be recorded without intrinsic intensifier noise, since during this time the probability that either single electrons or electron groups will leave the entrance photocathode is very small. However, this condition is realized only if we supply the voltage to the entrance chamber simultaneously with the passage of the particle through a scintillator or radiator, i.e., synchronously.

Estimates show that the synchronized supply of the entrance chamber from scintillation counters or Cerenkov counters is limited by the delays of the controlling signal in the electronic control circuits if the duration of the light flashes in the scintillators is less than 10^{-8} sec.

Therefore arrangements have been proposed [1,2,6,10,19] for synchronized pulse supply of the amplifier chambers of an image intensifier and a continuously operating state of the entrance chamber. In this case the optical image of the object being studied passes through the entrance chamber and is stored in the fluorescent screen for the decay time of the phosphor. Transfer of the optical image from the entrance-chamber screen to the output screen of the intensifier is accomplished with synchronized pulse supply of the amplifier chambers.

The number of noise light flashes at the output screen of the intensifier will be determined in this case by the duration of the pulse. In fact, from the expression

$$m = N_0(1 - e^{-t/\tau_0}), \qquad (4)$$

in which N_0 designates the number of excited molecules of the phosphor and m—the number of molecules which radiate in a time t, it is evident that to decrease the number of noise light flashes at the output screen it is necessary to transfer the optical image of the object from the entrance chamber to the amplifier chambers in a time interval t less than the decay time τ_0 of the fluorescent screen. This is possible only under the condition that the duration of the optical image being intensified is many times less than the decay time of the fluorescent screen. However, with pulsed supply of the image intensifier chambers, both the number of noise light flashes at the output screen and the brightness of the optical image of the object being photographed are reduced, since the gain of the apparatus is not utilized completely. This statement is valid for image intensifiers whose fluorescent screens have equal or nearly equal decay times.

Figure 5 shows a block diagram of a synchronized pulse supply for the first amplifier chamber of an

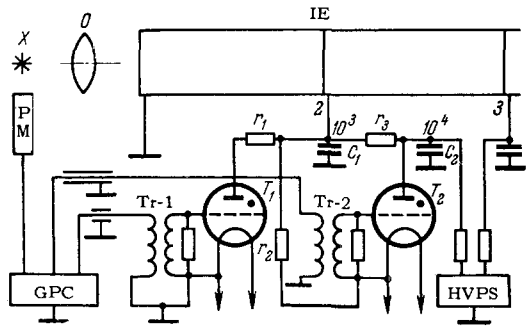

FIG. 5. Schematic diagram of synchronized pulse supply for the first amplifier chamber of an image intensifier. X – object under study; O – Objective; EI – Image intensifier; PM – photomultiplier; GPC – gate pulse circuit; HVPS – high voltage power supply.

image intensifier.[19] In the initial state the image intensifier photocathode is grounded and a high voltage, positive polarity pulse is supplied to the screens of the entrance chamber 2 and the first amplifier chamber 3. If the potentials on these screens are equal, the entrance chamber is in its operating state and the first amplifier chamber is turned off. As a result the optical image of the object being studied passes through the entrance chamber and is stored in the screen of the entrance chamber for a time interval equal to the decay time of the phosphor.

The image is transferred from the screen of the entrance chamber to the output screen of the image intensifier only on removal of the voltage from the entrance-chamber screen. As a result of this operation the first amplifier chamber transfers to the operating state, since a potential difference appears between the photocathode and screen of this chamber, and the entrance chamber is turned off for receiving new events, since the photocathode and screen of this chamber are at the same potential.

Removal of voltage from the entrance-chamber screen is accomplished by a control pulse synchronized with the object being studied. It is fed to the input of a trigger-pulse circuit which produces two pulses displaced in time. The first pulse is fed to the grid of thyratron T_1 and fires it. As a result capacitor C_1 is discharged to ground and removes the voltage from the entrance-chamber screen. The second trigger pulse, after a time interval t, is fed to the grid of thyratron T_2 and fires it. Capacitor C_1 is changed to the necessary voltage and the image intensifier transfers to the initial state.

By way of illustration, Fig. 6 shows photographs of the high-frequency electron-optical scanning of a spark discharge in a counter.[19] Photograph a) was obtained with dc supply voltage for the image intensifier, and photograph b) for pulsed supply of the first amplifier chamber with a duration of 80 $\times 10^{-6}$ sec. It is evident from the photographs of Fig. 6 that the intrinsic noise of the intensifier is almost completely suppressed in the pulsed operation of the first amplifier chamber. We will observe that pulsed supply of the chambers of an image intensifier is used in programming the operation of scintillation chambers and Cerenkov chambers.

II. SCINTILLATION CHAMBERS

In the study of interactions of high-energy particles with nucleons and nuclei it is desirable to use detectors whose principle of operation would permit programming these investigations. Such a detector is the scintillation chamber, which consists of a scintillator, an image intensifier, and controlling counters.

The choice of scintillator is determined mainly by the physical problem to be solved with a given detector. Some investigations have utilized a scintillation chamber with a homogeneous working volume.[10,20,63,64] In such a detector the entire volume of the scintillator is not used, buy only a small part determined mainly by the viewing angle and the focal length of the objective.

The efficiency of the optical systems which project the particle tracks from the scintillator to the entrance photocathode of the image intensifier does not exceed a few per cent. Therefore in development of scintillation chambers particular attention is devoted to the problem of coupling the working volume to the entrance photocathode of the image intensifier.

FIG. 6. High-frequency electron-optical scanning of a spark discharge in a counter. The photographs were obtained with continuous voltage supply to the amplifier chambers (a) and with pulsed supply (b).

Table I

Scintillator	Relative pulse height	Decay time, sec	Peak of emission spectrum, Å	Hydrogen content, %	Density, g/cm³
NaI(Tl)[24]	1	$2.5 \cdot 10^{-7}$	4100	–	3.67
CsI(Tl)[25]	0.75	$1 \cdot 10^{-6}$	white	–	4.5
Anthracene[26–28]	0.50	$2.7 \cdot 10^{-8}$	4400	46	1.25
Stilbene	0.26	$8 \cdot 10^{-9}$	4100	46	1.16
Tolane	0.25	$7 \cdot 10^{-9}$	3900	44	1
Naphthalene + 1% anthranilic acid [29]	0.25	$2 \cdot 10^{-8}$	4060	44	1.1
Solution of 3 g/l terphenyl + 100 ml/l POPOP in toluene	0.20	$2 \cdot 10^{-9}$	4200	53	0.87
2% terphenyl + 0.02% POPOP in polystyrene [30,31]	0.20	$2 \cdot 10^{-9}$	4250	50	1

Reynolds and Condon [21] and Savchenko [23] have proposed scintillation chambers with filament scintillators.

4. Characteristics of Some Scintillator Materials

The main requirements imposed on the scintillator materials from which the working volume of a scintillation chamber is prepared are the following:

a) high light output;

b) short duration of light flash;

c) high transparency of the scintillator material for its own radiation;

d) correspondence of the spectral composition of the light flash to the spectral sensitivity of the entrance photocathode of the intensifier.

The characteristics of several scintillator materials are listed in Table I.

It follows from the data of Table I that homogeneous working volumes for scintillation chambers can be prepared both from single crystals and from liquid and plastic scintillators. The light output of these scintillators is sufficient to form an optical image of a particle-track projection on the entrance photocathode of the image intensifier.

A good material for preparation of scintillator filaments is plastic scintillator containing 2% terphenyl + 0.02% POPOP in polystyrene.[39]

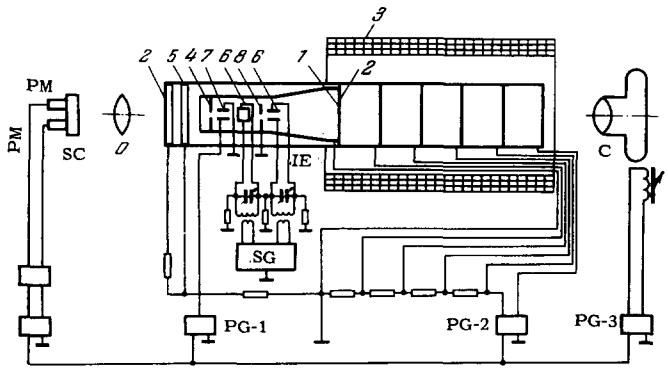

FIG. 7. Diagram of a scintillation chamber. SC – scintillator crystal; O – objective; 1 – fluorescent screen; 2 – photocathode; 3 – solenoid; 4 – diaphragm; 5 – focusing electrode; 6 – deflecting plates; 7, 8 – pulsed electron gate; C – camera; PG-1 – electron gate pulse generator; PG-2 – high voltage pulse generator; PG-3 – camera control pulse generator; SG – sweep generator.

5. Scintillation Chambers With a Homogeneous Working Volume

Passage of a charged particle though a scintillator is accompanied by formation of a luminous track in which the number of photons depends on the energy E dissipated by the particle in the scintillator and the energy E_p expended in producing one photon.

The number of luminous points per cm in the track projection of a relativistic particle can be determined from the expression

$$m = \frac{\eta \frac{E}{E_p}}{16n^2} B^2 \frac{K^2}{(1+K)^2}. \quad (5)$$

Here η is the quantum efficiency of the entrance photocathode of the intensifier and n is the refractive index of the scintillator material; B and K are the relative aperture and magnification of the objective.

Estimates which have been made show that the value of m does not exceed 12 and is roughly equal to the number of points in the relativistic-particle track projection obtained in bubble chambers.

The scintillation chamber described by Zavoĭskiĭ et al.[1,2] consisted of a single crystal of CsI(Tl), a multistage image intensifier, and a camera. Images of particle tracks in the crystal were projected by a fast objective onto the entrance photocathode of the intensifier, which was operated in the pulsed mode. A block diagram of the chamber is shown in Fig. 7.

A charged particle which hit the crystal excited light flashes which were recorded by two photomultipliers operating in coincidence. The resulting pulse was amplified and fed to a circuit which controlled

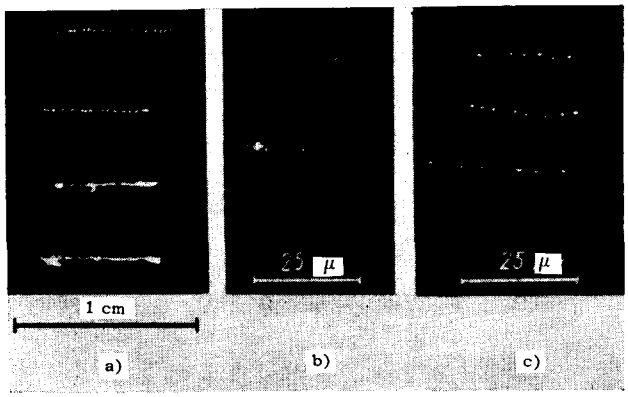

FIG. 8. Photographs of particle tracks: a) protons with E ~ 200 MeV in CsI(Tl); b) α particles with E = 5.2 MeV in CsI(Tl); α particles with E = 5.2 MeV in anthracene.

the gating pulses for the entrance and output chambers of the intensifier. The duration of the entrance-chamber pulse did not exceed 3×10^{-6} sec. As a result the intrinsic noise of the intensifier was completely suppressed.

As an illustration Fig. 8 shows photographs of tracks of protons with a kinetic energy of ~200 MeV and α particles in crystals of CsI(Tl) and anthracene. Since the range of 5.2-MeV α particles does not exceed a few tens of microns, the tracks were photographed through a microscope with a magnification of 200.

Examination of the photographs in Fig. 8 shows that the structure of the tracks in the CsI(Tl) crystal depends on the energy dissipated by the particles in the scintillator. In those cases when the particle dissipates its entire energy in the crystal, the tracks are continuous. With increasing kinetic energy, the ionization loss of the particle decreases and the tracks change from continuous to discrete, i.e., consisting of individual luminous points. The discontinuities in the track are due to statistical fluctuations of the light quanta.

It is of considerable interest to study the detection of particle tracks with minimum ionization. Such studies have been made both in cosmic rays and in particle beams from accelerators.[10,20,35,63,64]

Demidov and Fanchenko[10] have described attempts to detect tracks of relativistic cosmic-ray particles. The chamber utilized a NaI(Tl) crystal which, with a 115-g/cm^2 block of lead, was placed between two scintillation counters connected in coincidence to select the direction of the cosmic rays. The image intensifier was operated in the pulsed mode. The chamber was controlled by the scintillation counters. The pulse length was 10^{-4} sec. The optical image of the particle tracks was photographed from the output screen of the intensifier onto motion-picture film. A photograph of a relativistic-particle track in the NaI(Tl) crystal is shown in Fig. 9a.

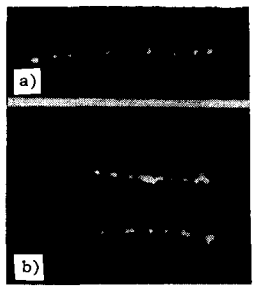

FIG. 9. Photographs of the tracks of relativistic particles in a crystal of NaI(Tl): a) cosmic-ray particles; b) 2-BeV/c π meson.

Jones, Perl, and co-workers[20,33-35] have described a scintillation chamber which they operated in 2-BeV/c π-meson beams. The working volume of the chamber consisted of a $50 \times 50 \times 100$ mm NaI(Tl) crystal. The optical image of the particle tracks was amplified by several image intensifiers, of which the second and last were pulsed. Scintillation counters were used to control the intensifiers. The pulse duration was 2—15 μsec in the second intensifier and 1—15 msec in the final intensifier. Figure 9b shows tracks of 2-BeV/c π mesons obtained in this way.

Examination of the photographs of particle tracks obtained in scintillation chambers with a homogeneous working volume shows that these detectors have satisfactory geometrical resolution. However, their application is limited by the small working volume.

6. Scintillation Chamber With Filament Scintillators

The working volume of this type of scintillation chamber is prepared from optically transparent scintillator filaments. The filaments are arranged in rows, the ends of the filaments in the even rows being rotated 90° with respect to the ends of the filaments in the odd rows. A particle track in such a scintillator is reproduced by the light from the ends of the filaments through which the particle passed. The actual trajectory of a particle which has passed through a filament scintillator is reconstructed from two orthogonal projections.[6,42-48,65]

In most cases the filament scintillator is used in optical contact with the entrance photocathode of an image intensifier. As a result the geometrical width of the track is determined by the diameter of the filaments of which the scintillator is prepared. To obtain high geometrical resolution it is desirable that the working volume of the scintillation chamber be prepared from scintillator filaments of the smallest possible diameter d_0, which can be estimated from the expression

$$d_0 = \frac{E_p}{\eta K E}. \qquad (6)$$

Here E is the energy lost by the particle per cm of path and K is the fraction of the light which reaches

the end of the filament and consequently the entrance photocathode of the amplifier. For plastic scintillators $E_p \sim 100$ eV[32] and $E \cong 2$—2.5 MeV. For $K = \eta = 0.1$ the minimum filament diameter does not exceed 0.006 mm. Preparation of scintillator filaments of this diameter involves definite technical problems associated with the properties of the material.[22,23,36] Isaev et al.[39] have described a technique for preparing scintillator filaments 0.3—5 mm in diameter and 1000—1200 mm long. Transparent and elastic filaments without air bubbles have been obtained from plastic scintillator containing 2% terphenyl + 0.02% POPOP in polystyrene, made by the method described by Koton et al.[40]

The transparency of scintillator filaments to their own radiation[39,41,43] is a problem of considerable interest. Isaev et al.[39] have studied the transparency of filaments made from plastic scintillator containing 2% terphenyl + 0.02% POPOP in polystyrene. They measured the pulse heights at the photomultiplier output as a function of the location at which the filament was irradiated by a collimated beam of Co^{60} γ rays. The attenuation of the pulse height in a 480-mm length of filament was 35% and did not depend on the filament diameter. On the basis of these results we can expect that scintillation chambers with filament scintillators can be prepared with working volumes up to a cubic meter.

The threshold sensitivity of a scintillation chamber with a filament scintillator, determined from the expression

$$E_0 = \frac{E_p}{\eta K}, \qquad (7)$$

is about 10—15 keV. This value agrees satisfactorily with the value 40—60 keV obtained from analysis of relativistic-particle tracks recorded in a scintillation chamber with a filament scintillator. Consequently such a detector will record even charged particles whose range is less than the diameter of the scintillator filaments. This low threshold sensitivity of a filament scintillation chamber makes it a promising detector for studying elastic scattering at small angles, both of relativistic and strongly ionizing particles and of neutrons and γ rays.

Figure 10 shows photographs of relativistic-particle tracks obtained in a filament scintillation chamber.[50] Study of these photographs shows that the geometrical width of the particle tracks considerably exceeds the diameter of the scintillator filaments. The smearing of particle tracks in a filament chamber is evidently due to the large thickness of the glass at the entrance photocathode of the image intensity and to illumination of neighboring filaments. The latter effect can be reduced to a minimum by placing black paper between the layers of scintillator filaments.

The particle track widths obtained in a filament chamber do not limit the application of this type of detector in recording elastic and inelastic interactions of nuclear radiation with matter.[66-70]

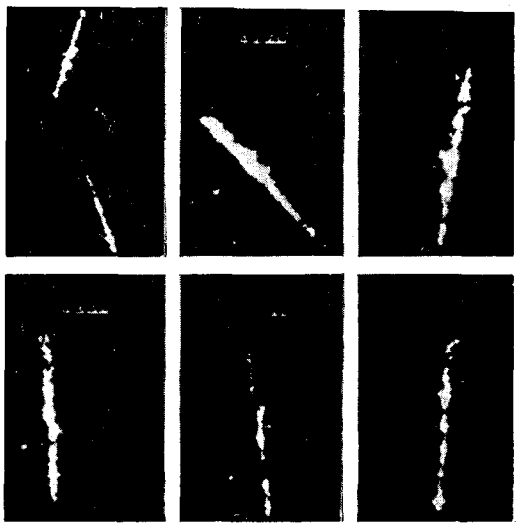

FIG. 10. Photographs of the tracks of relativistic particles in a scintillation chamber with filament scintillators.

7. Some Applications of Filament Scintillation Chambers

Filament scintillation chambers have been used by several investigators to study a variety of physical problems. We will discuss several of these.

a) Determination of the geometry of charged-particle beams produced in accelerators. Waters et al.[49] have described an apparatus for determining the geometry and composition of 735-MeV/c charged-particle beams which have been produced in an accelerator and passed through a separator. It consists of a filament scintillator, an image intensifier, and a television system (Fig. 11).

A filament scintillator 125 mm in diameter and 31 mm long was prepared from filaments 0.75 mm in diameter. It was in optical contact with the entrance photocathode of a single-stage image intensifier. An optical image of the beam configuration was displayed on the television screen.

b) Study of the decay of B_5^{12}. Reynolds et al.[50] have described a scintillation chamber in which the

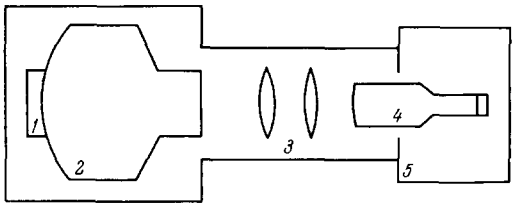

FIG. 11. Diagram of apparatus for determining the geometry of particle beams. 1 – filament scintillator; 2 – single-stage intensifier; 3 – lenses; 4 – image intensifier; 5 – television system.

filament scintillator simultaneously serves as the target for study of the reaction

$$\mu^- + C_6^{12} \longrightarrow B_5^{12} + \nu. \qquad (A)$$

The working volume of the chamber was prepared of scintillator filaments 0.5 mm in diameter and 75 mm long. It was in the form of a cylinder optically divided into three parts. The scintillator was in optical contact with the entrance photocathode of an image intensifier. Operation of the chamber was controlled by scintillation counters. A block diagram of the equipment is shown in Fig. 12.

It was established by analyzing 800 photographs with decay of a B_5^{12} nucleus that the lifetime of this nucleus is 27×10^{-3} sec. The decays of a μ meson and a B_5^{12} nucleus are illustrated by the photographs in Fig. 13. The points of decay of the μ^- meson and the B_5^{12} nucleus are marked in the photographs by two fiducial points along the vertical direction, obtained by illumination of individual filaments.

With a change in the construction of the chamber working volume, Reynolds et al. studied the decay scheme of the π^+ meson:

$$\pi^+ \longrightarrow \pi^0 + e^+ + \nu. \qquad (B)$$

c) Measurement of the angular distribution of charged particles in a given solid angle. Butslov et al.[51] describe a method for measuring the angular distribution of charged particles in a given solid angle by means of a filament scintillation chamber. The principle of the method is as follows: if the direction of motion of a particle coincides with a selected direction of the filament scintillator, its passage through a scintillator filament is recorded in the form of a single luminous point.

If the particle passes through the filament scintillator at an angle α the number of luminous flashes will correspond to the number of filaments through which the particle has passed. By measuring the projection of the track, it is easy to find the angle α, i.e.,

$$\operatorname{tg}\alpha = \frac{b}{l}, \qquad (8)$$

where b is the track projection and l is the length of the filament scintillator.

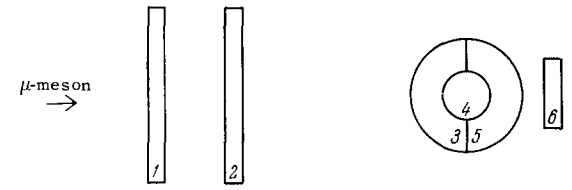

FIG. 12. Arrangement for controlling a scintillation chamber. 1, 2, 6 – scintillation counter; 3, 4, 5 – filament scintillators placed in optical contact with an image intensifier and photomultipliers.

The method has been tested experimentally in a setup consisting of a filament scintillator, an image intensifier, a camera, and a scintillation counter.

The filament scintillator was assembled from filaments 0.5 mm in diameter and 50 mm long. The construction of the scintillator prevented passage of light from a given filament to its neighbors. The filament scintillator was placed in a vertical plane. One plane of filament ends was projected onto the image intensifier photocathode by means of a mirror and lens, and the second plane was viewed by the cathode of a photomultiplier. The scintillation counter utilized a plastic scintillator 40 mm in diameter.

In these experiments the image intensifier operated in the pulsed mode and programming control was accomplished by scintillation counters operating in coincidence.

The experimental data obtained confirmed the accuracy of the proposed technique.

III. CERENKOV CHAMBER

In studies carried out with particle beams produced in accelerators, problems often arise of detecting particles with a definite velocity. Of all types of detectors, only Cerenkov angular counters permit direct measurement of particle velocity.

For the determination of velocities and direction of particles over a wide range of energies, a detector has been proposed which consists of a radiator, an image intensifier, a camera, and controlling counters.[52,53,58] This detector is based on Cerenkov

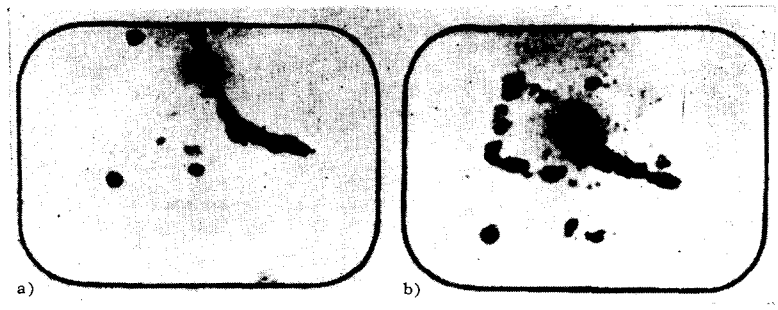

FIG. 13. Photographs of the decay of a) a μ meson, and b) a B_5^{12} nucleus.

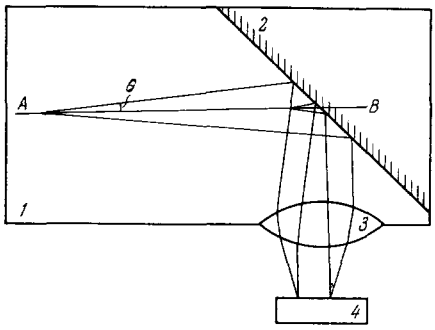

FIG. 14. Diagram of Cerenkov chamber. 1 – radiator; 2 – mirror; 3 – lens; 4 – image intensifier.

radiation and we therefore suggest that it be called a Cerenkov chamber.*

8. Description of the Method

Let a charged particle move along the line AB through the Cerenkov chamber shown schematically in Fig. 14. If the particle velocity βc is greater than the phase velocity of light in the radiator material, $u = c/n(\nu)$, Cerenkov radiation will occur in the material. A characteristic feature of this radiation is its strikingly directional nature. According to the theory developed by I. E. Tamm and I. M. Frank,[54] the direction of the radiation forms an angle θ with the direction of the radiating particle, where θ is determined by the relation

$$\cos\theta = \frac{1}{n\beta}, \tag{9}$$

where $\beta c = v$ is the particle velocity, and n is the refractive index of the radiator material.

The Cerenkov radiation passes through an optical system and is collected at the focal plane in a ring whose radius r is related to the angle of the radiation by the expression

$$r = f\tan\theta, \tag{10}$$

where f is the focal length of the optical system. This ring can be considered as an "image" of the particle, i.e., as a source of light the particle is equivalent to an infinitely distant ring.

By measuring the radius of the Cerenkov ring, we find the angle θ and consequently the particle velocity. The resolution of a Cerenkov chamber for particle velocity is determined by the accuracy of measuring the radius of the ring and by the smearing of the radiation angle θ:

$$\frac{d\beta}{\beta} = \frac{r^2}{r^2+f^2}\frac{dr}{r}, \tag{11}$$

and

$$\frac{d\beta}{\beta} = \frac{r}{f}d\theta. \tag{12}$$

The geometrical resolution of multistage image intensifiers permits measurement of the ring radius with an accuracy of 0.1 mm. This provides a velocity resolution for the particles of $d\beta/\beta \sim 10^{-5}$.

The smearing of the Cerenkov radiation angle is due to energy losses of the particles in the radiator, to diffraction effects and multiple scattering, and also to the dispersion of the radiator material. The greatest contribution to the smearing of the angle is from the latter effect.[55-57]

The dependence of the particle velocity on the radiator material dispersion has the form

$$\frac{d\beta}{\beta} = \frac{dn}{n}. \tag{13}$$

Estimates which have been made show that $d\beta/\beta$ amounts to about 10^{-5} for gaseous radiators and $(3-5)\times 10^{-3}$ for radiators of condensed media.

9. Radiator Materials and the Size of the Working Volume

Measurements of particle velocity from the Cerenkov-radiation ring radius impose definite requirements on the radiator material and on its working length: first, that the radiator material be transparent both for visible light and for the near ultraviolet; second, that it have a very small dispersion and be optically homogeneous; third, that it have low density, in order to reduce ionization loss to a minimum, and low atomic number in order to reduce the angular smearing of the radiation cone due to multiple scattering.

These requirements are fulfilled most completely by gases. However, because of the low refractive indices of gases, the intensity of the Cerenkov radiation is no greater than 0.5—1 photon per cm of particle path. By using compressed gases in the working volume, we can bring the intensity of the radiation up to 10—15 photons per cm of particle path. However, this will also increase the dispersion of the material. Table II lists the refractive indices of several gases at various pressures.

It follows from the data of Table II that the most suitable material for a radiator is propane or pentane. In fact, a refractive index of 1.01 can be obtained at a gas pressure of 10—12 atm.

Of the solid and liquid dielectrics, distilled water and clear plastic satisfy these requirements to some degree. Specifically, water, whose refractive index is n = 1.334, has the best transparency for visible light and the near ultraviolet and contains up to 70% hydrogen. In addition, the change of refractive index in the region of the maximum spectral sensitivity of an antimony-cesium photocathode that does not exceed 4×10^{-3}. The optical characteristics of clear plastic are not very different from those of distilled water.

*The name actually proposed by the author is Vavilov-Cerenkov chamber.–Translator.

Table II

Material	Refractive index			
	At 1 atm, 0°C	At 14 atm, 25°C	At the critical point	In the liquid state
Hydrogen	1.000138	—	—	1.097—253° C
Helium	1.000036	1.00046	—	1.0206—4.22° K 1.0269—2.26° K
Nitrogen	1.000296	1.00381	—	1.205—190° C
Air	1.0003	—	—	—
Carbon dioxide gas	1.000415	1.0060	1.0264, 25° C, $P=63.5$ atm	—
Ethane	1.0007	1.0099	1.0263, 25° C, $P=37.3$ atm	
Propane	1.001	—	1.009, 22° C, $P=9$ atm	1.19—1.23
Freon 13-B-1	1.000864	1.0153	1.0153	—
Ethyl ether	1.00152	—	42° C, $P=14.3$ atm 1.00136	—
Pentane	1.00171	—	34.6° C, $P=1$ atm —	—
Argon	1.000281	1.00360	—	—
Methane	1.000441	—	—	—

Detection of the Cerenkov-radiation ring from a single particle on film is possible only for a definite intensity of radiation. The number of photoelectrons m_e from Cerenkov radiation excited by a charged particle per cm of path in the radiator can be determined from the expression [57]

$$\frac{dm_e}{dL}=\frac{2\pi}{137}\xi\eta\left(1-\frac{1}{n^2\beta^2}\right)\int S(\lambda)\frac{d\lambda}{\lambda^2}, \qquad (14)$$

in which ξ designates the efficiency for collection of light at the entrance photocathode of the image intensifier, and η and $S(\lambda)$ are respectively the quantum efficiency of the photocathode and its relative spectral characteristic.

If we assume that the image intensifier permits recording on the film of the light flash from a single photoelectron, then, corresponding to a number of photoelectrons m_e, there will be m_e luminous points in the Cerenkov-radiation ring. For example, in a radiator whose refractive index is n = 1.006, a charged particle with $\beta = 0.999$ will produce roughly 0.32 luminous points per cm of path. This value is obtained for the conditions $\xi = 0.7$, $\eta = 0.1$, and $S(\lambda)\frac{d\lambda}{\lambda^2} = 1.03\times 10^4$ in the wavelength region $\lambda = 3000$—6000 Å. With these assumptions the radiator length has been calculated as a function of $n\beta$ for production of a Cerenkov ring consisting of 32 luminous points. The results are shown in Fig. 15, which also shows the values of the angle θ as a function of $n\beta$.[53] The theoretical curves of Fig. 15 allow us to choose not only the length but also the refractive index of the material which will guarantee the detection of the Cerenkov ring on film.

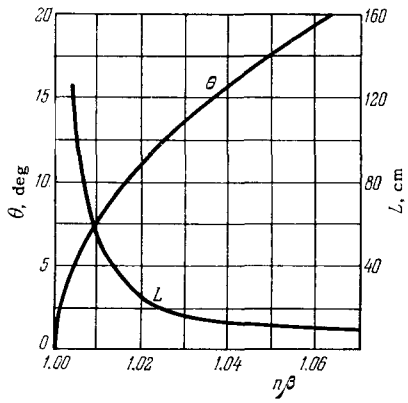

FIG. 15. Angle of Cerenkov radiation and length of radiator as a function of $n\beta$. The radiator length is calculated so as to produce a ring of 32 luminous points.

10. Detection of Cerenkov Rings from Single Relativistic Particles

Papers have been published which describe Cerenkov chambers for detection of the rings from single relativistic particles. We will discuss some of these papers.

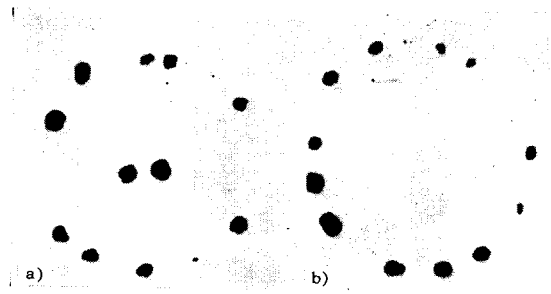

FIG. 16. Photographs of Cerenkov-radiation rings from single relativistic particles. a) radiator with filament scintillator. The point in the center of the ring corresponds to passage of the particle through the filament scintillator; the second point is background; b) cylindrical radiator with spherical lens.

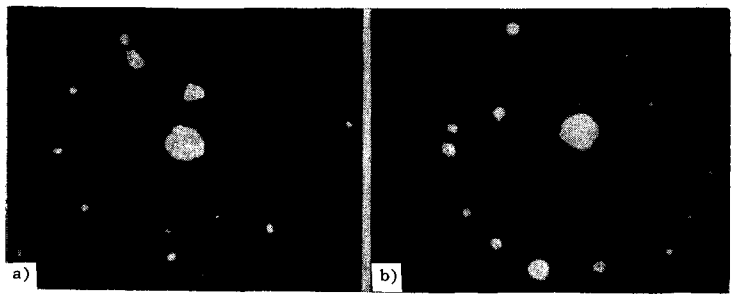

FIG. 17. Photographs of Cerenkov-radiation rings from an 820-MeV/c π meson: a) from a single π meson; b) from two π mesons.

Butslov et al.[59,60] have described a chamber for detection of Cerenkov rings from relativistic cosmic-ray particles. The chamber radiator was made of clear plastic. It was in the shape of a cylinder with a diameter of 30 mm and length of 150 mm, which was terminated in a cone with a lens on the end. The angle of the cone did not exceed 24°. The cone of the radiator had a cylindrical well 30 mm in diameter and 45 mm deep. The surface of the well was covered with a black lacquer. In the well was placed a filament scintillator made from filaments 0.5 mm in diameter and 50 mm long. The direction of the filaments coincided with the direction of the radiator axis.

The image intensifier was operated in the pulsed mode. Control was provided by scintillation counters which selected the direction of the cosmic-ray particles passing through the radiator and the filament scintillator. Figure 16 shows two photographs of Cerenkov-radiation rings from single relativistic particles. The luminous point at the center of the ring corresponds to passage of the particle through the filament scintillator. The ring consists of 12—15 luminous points.

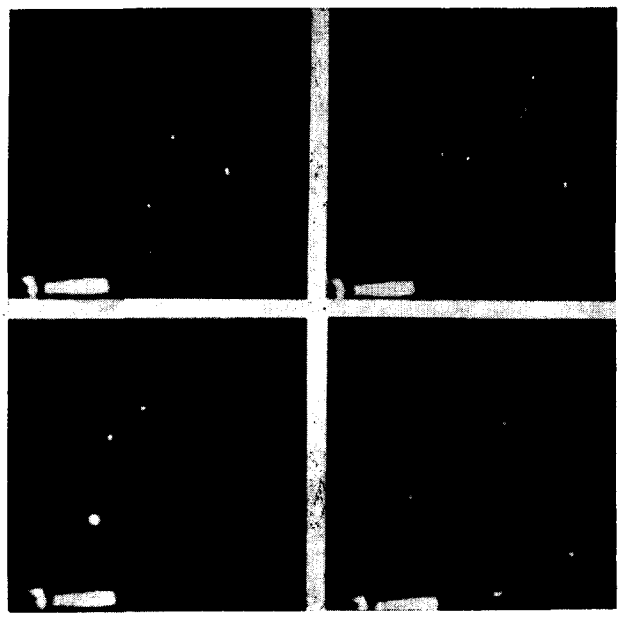

FIG. 18. Photographs of Cerenkov-radiation rings from single π mesons of 700 MeV/c in a gas radiator.

Poultney et al.[61] have described a Cerenkov chamber for determination of the velocity of 820-MeV/c π mesons. The chamber utilized a conical radiator of clear plastic 48 mm long. The angular opening of the cone was 19°.

Light rays from Cerenkov flashes excited by π mesons left the radiator at an angle of 14° and were collected by an optical system onto the entrance photocathode of the image intensifier, which was operated in the pulsed mode. Control was accomplished by two scintillation counters operating in coincidence. Figure 17 shows photographs of Cerenkov rings from 820-MeV/c π mesons. The ring consists of 5—6 luminous points. When two π mesons passed through the radiator, the number of points in the ring was increased by a factor of two (Fig. 17b). The authors explain the small number of points in the ring by the poor efficiency of the optical system ($\xi \sim 20\%$).

A Cerenkov chamber with a gaseous radiator has been described by Binnie et al.[62] The radiator material was Freon 13, whose refractive index at 18 atm was 1.021. The gas was in a container 90 mm in diameter and 850 mm long.

Light rays from Cerenkov flashes excited by 700-MeV/c π mesons were reflected from a mirror placed at 45° to the axis of the radiator, passed through a window, and were collected by a system of lenses into a ring of diameter 16 mm at the entrance photocathode of the image intensifier.

The image intensifiers were operated in the pulsed mode. Control was accomplished by two scintillation counters operating in coincidence.

Figure 18 shows photographs of Cerenkov rings from 700—MeV/c π mesons. In scanning the photographs, large fluctuations are observed both in the

radii of the rings and in the number and size of the luminous points. The authors explain these fluctuations by the large momentum spread of the π mesons and by the effects of ionization loss and multiple scattering. However, the principle cause is the statistical fluctuation in the small number of luminous points composing the ring.

Recording of the rings on film makes the use of Cerenkov chambers particularly promising for study of elastic scattering of high-energy particles at small angles, since the angular resolution of the particles in the chamber can be as small as $(1-5) \times 10^{-4}$ rad and does not depend on the angular spread of the particle beam.

[1] E. K. Zavoĭskiĭ, G. E. Smolkin, A. G. Plakhov, and M. M. Butslov, DAN SSSR 100, 241 (1955).

[2] E. K. Zavoĭskiĭ, M. M. Butslov, A. G. Plakhov, and G. E. Smolkin, Atomnaya énergiya, No. 4, 35 (1956).

[3] F. Eckart, Ann. Physik 14, 1 (1954).

[4] J. A. Jenkins and R. A. Chippedale, Brit. Inst. Radio Engng. 11, (11), (1951).

[5] M. P. Vanyukov, UFN 60 (2), 295 (1956).

[6] Yu. K. Akimov, M. M. Butslov, O. V. Savchenko, and L. M. Soroko, Atomnaya énergiya 12, 413 (1962).

[7] J. D. McGee, Proc. of the Symp. on Nucl. Inst., Harwell, September, 1961, p. 1.

[8] P. V. Shcheglov, Élektronnaya teleskopiya, (Electronic Telescopy), Fizmatgiz, 1963.

[9] E. K. Zavoĭskiĭ, M. M. Butslov, and G. E. Smolkin, DAN SSSR 111, 996 (1956), Soviet Phys. Doklady 1, 743 (1957).

[10] B. A. Demidov and S. D. Fanchenko, JETP 39, 64 (1960), Soviet Phys. JETP 12, 46 (1961).

[11] R. G. Stoudenheimer, J. C. Moor, and H. L. Palmer, IRE Trans. Nucl. Sci. 7, No. 2-3, 136 (1960).

[12] W. L. Wilcock, D. L. Emberson, and B. Weekley, IRE Trans. Nucl. Sci. 7, No. 2-3, 126 (1960).

[13] A. E. Anderson, IRE Trans. Nucl. Sci. 7, No. 2-3, 133 (1960).

[14] R. Engstrom, J. Opt. Soc. Amer. 37, 420 (1947).

[15] B. T. Brezhnev, JETP 17, 2 (1947).

[16] P. I. Lukirskiĭ, Izv. AN SSSR, ser. fiz. 10, 309 (1946).

[17] S. F. Essig, Advances in Electronics and Electron Physics 12, 73 (1960).

[18] V. I. Krasovskiĭ, USSR Inventor's Certificate No. 55354, June 19, 1939.

[19] G. E. Smolkin, PTÉ, No. 4, 60 (1957).

[20] L. W. Jones, K. Lai, R. Newsome, and M. L. Perl, IRE Trans. Nucl. Sci. 7, No. 2-3, 145 (1960).

[21] G. T. Reynolds and P. E. Condon, Rev. Sci. Instr. 28, 1098 (1957).

[22] G. T. Reynolds, Nucleonics, 16, No. 6, 60 (1958).

[23] O. V. Savchenko, PTÉ, 4, 142 (1959).

[24] J. B. Birks, Scintillation Counters, Pergamon Press, London, 1953.

[25] R. Hofstadter, Nucleonics 6, No. 5, 70 (1950).

[26] F. B. Harrison, Nucleonics 10, No. 6, 40 (1952).

[27] G. G. Kelley and M. Goodrich, Phys. Rev. 77, 138 (1950).

[28] W. A. Little and J. B. Birks, SAAAS Congress, Cape Town, July, 1952.

[29] G. S. Belikova, L. M. Belyaev, and Kh. V. Protopopov, Stsintillyatory i stsintillyatsionnye materialy (Scintillators and Scintillation Materials), Moscow, 1960.

[30] M. N. Medvedev, E. N. Matveeva, and L. Ya. Zhil'tsova, PTÉ, 1, 55 (1957).

[31] E. N. Matveeva, M. N. Medvedev, and M. D. Shafranov, Izv. AN SSSR, ser. fiz. 23, 108 (1959), transl. Bull Acad Sci. Phys. Ser. p. 105.

[32] E. A. Andreeshchev and I. M. Rozman, Optika i spektroskopiya 5, 39 (1958).

[33] M. L. Perl and L. W. Jones, Phys. Rev. Letters 2, 116 (1959).

[34] L. W. Jones and M. L. Perl, Conf. on High Energy Accel. and Inst., CERN, 561 (1959).

[35] L. W. Jones and M. L. Perl, Nucl. Inst. and Methods 10, 348 (1961).

[36] V. G. Kokoulin, PTE, 4, 183 (1963).

[37] P. A. Tove, Rev. Sci. Instr. 27, 143 (1956).

[38] R. M. Weinstein and H. V. Bradt, Rev. Sci. Instr. 30, 206 (1959).

[39] A. S. Isaev, M. N. Medvedev, and V. I. Prokhorov, Stsintillyatory i stsintillyatsionnye materialy (Scintillators and Scintillation Materials), Proceedings of Conf., Khar'kov, 1963.

[40] M. M. Koton, Yu. P. Panov, A. N. Pisarevskiĭ, and T. V. Timofeva, PTÉ, No. 1, 49 (1957).

[41] R. J. Potter and R. E. Hopkins, IRE Trans. Nucl. Sci. 7, No. 2-3, 150 (1960).

[42] G. T. Reynolds, R. Giaconi, and D. Scarl, Rev. Sci. Instr. 30, 497 (1959).

[43] K. Lande, A. K. Mann, M. M. Schlacter, D. M. Skyrme, and H. Uto, Rev. Sci. Instr. 30, 496 (1959).

[44] L. W. Jones and M. L. Perl, Rev. Sci. Instr. 29, 441 (1958).

[45] R. J. Potter and R. E. Hopkins, J. Opt. Soc. Amer. 49, 1128 (1959).

[46] K. Lande, A. K. Mann, K. Reibel, and D. H. White, IRE Trans. Nucl. Sci. 7, No. 2-3, 121 (1960).

[47] G. T. Reynolds, IRE Trans. Nucl. Sci. 7, No. 2-3, 115 (1960).

[48] G. T. Reynolds, R. A. Swanson, and D. B. Scarl, Rev. Sci. Instr. 31, 1011 (1960).

[49] J. R. Waters, G. T. Reynolds, D. B. Scarl, and R. A. Zdanis, Nucl. Inst. Methods 17, 44 (1962).

[50] G. T. Reynolds, D. B. Scarl, R. A. Swanson, J. R. Waters, and R. A. Zdanis, Proc. Symp. Nucl. Inst., Harwell, September, 1961, p. 24.

[51] M. M. Butslov, M. N. Medvedev, and V. M. Sheshunov, Nucl. Inst. Methods 20, 242 (1963).

[52] A. Roberts, Rev. Sci. Instr. 31, 579 (1960).

[53] A. Roberts, Nucl. Inst. Methods 9, 55 (1960).

[54] I. E. Tamm and I. M. Frank, DAN SSSR 14, 109 (1937).
[55] K. G. Dedrick, Phys. Rev. 87, 891 (1952).
[56] P. A. Cerenkov, DAN SSSR 20, 653 (1938).
[57] J. V. Jelley, Cerenkov Radiation and its Applications, Pergamon Press, New York, 1958.
[58] W. Kernan, A. Roberts, et al., Proc. of Intern. Conf. on Instrum. for High Energy Physics, New York, Interscience, 1961, p. 93.
[59] M. M. Butslov, M. N. Medvedev, P. I. Filippov, I. V. Chuvilo, and V. M. Sheshunov, Atomnaya énergiya 12, 412 (1962).
[60] M. M. Butslov, M. N. Medvedev, I. V. Chuvilo, and M. Sheshunov, Nucl. Inst. Methods 20, 263 (1963).
[61] S. K. Poultney, G. T. Reynolds, and J. R. Waters, Rev. Sci. Instr. 33, 574 (1962).
[62] D. Binnie, M. R. Jane, J. A. Newth, D. C. Potter, and J. Walters, Nucl. Instr. Methods 21, 81 (1963).
[63] O. Gildemeister and R. Giese, Nucl. Instr. Methods 20, 233 (1963).
[64] D. Binnier, M. R. Jane, J. A. Newth, D. C. Potter, and J. Walters, Nucl. Instr. Methods 20, 221 (1963).
[65] K. Lande, A. K. Mann, and D. H. White, Nucl. Instr. Methods 20, 245 (1963).
[66] J. M. Dobbs, K. Lande, A. K. Mann, K. Reibel, F. J. Sciulli, H. Uto, D. H. White, and K. K. Young, Phys. Rev. Letters 8, 295 (1962).
[67] International Conference on High Energy Accel. and Inst., CERN, Geneva, 1959.
[68] IRE Trans. Nucl. Sci. 9, No. 3 (1962).
[69] Proc. of the Sympos. on Nucl. Instr., Harwell, September, 1961.
[70] Instrumentation for High Energy Physics, Nucl. Inst. Methods 20, (1963).

Translated by C. S. Robinson